Pergamon

Tetrahedron: *Asymmetry* 13 (2002) 475–489

TETRAHEDRON: *ASYMMETRY*

Computational studies on the enantioselectivity of α-chymotrypsin towards β-carbomethoxy-γ-lactams

F. Felluga,[a] M. Fermeglia,[b] M. Ferrone,[b] G. Pitacco,[a] S. Pricl[b,*] and E. Valentin[a]

[a]*Department of Chemical Sciences, University of Trieste, Via Giorgeri 1, 34127 Trieste, Italy*
[b]*Computer-aided Systems Laboratory, Department of Chemical, Environmental and Raw Materials Engineering-DICAMP, University of Trieste, Piazzale Europa 1, 34127 Trieste, Italy and ICS-UNIDO, Area Science Park, Padriciano 99, 34100 Trieste, Italy*

Received 31 January 2001; accepted 15 March 2002

Abstract—In our previous work, racemic β-carbomethoxy-γ-lactams were subjected to enzymatic hydrolysis in the presence of α-chymotrypsin. The hydrolysis of three *N*-substituted lactams proved to be highly enantioselective, whereas an unsubstituted lactam was recovered in racemic form. Thus, in this paper we applied several molecular modeling protocols to explain the substrate specificity and the enantioselectivity of this enzyme. The adopted procedures involved accurate docking experiments of both enantiomers of each lactam to the protein active site, whose 3-D structure was obtained from X-ray crystallographic data, followed by extensive conformational and energetic analysis of the computer-generated complexes. The results obtained fully account for the experimental evidences on the enantioselective hydrolysis of these interesting, potential drugs by α-chymotrypsin.

1. Introduction

Enzymes play a major role in organic synthesis as environmentally friendly catalysts for a wide range of chemical transformations.[1,2] Among this plethora of biomacromolecules, hydrolytic enzymes are particularly useful as they exhibit broad substrate specificities and can induce high enantioselectivities, are commercially available, and do not necessitate the use of expensive and/or unstable coenzyme systems. To date, esterolytic enzymes, such as lipases and proteases, appear to be the most widely employed in organic processes. For an enzyme to gain extensive application, the factors governing its specificity, particularly the relationships between its selectivity and the structural features of the substrate it processes, must be understood. Accordingly, several simple and easy-to-use active site models have been proposed for a number of different esterases,[3,4] and some well defined SARs (structure–activity relationships) are emerging.

Rather recently, straightforward models for enzyme selectivity, known as rules, have been proposed in the literature for some popular lipases such as *Pseudomonas cepacia* (PCL),[5,6] *Candida rugosa* (CRL),[7,8] and *Rhizomucor miehei* (RML).[9] Nonetheless, these types of models are limited to isosteres of known substrates, and can only predict which the fastest reacting enantiomer is. Therefore, the goals of more accurate modeling in this field should be at least threefold: (i) to explain, on a molecular level, the known behavior of an enzyme; (ii) to suggest how to change the selectivity of a reaction by modification of substrate, enzyme or reaction conditions, and (iii) to predict quantitatively the degree of stereoselectivity of an enzyme-catalyzed reaction.

In the last decades, X-ray data of a great number of enzymes have become available to the scientific community by means of public data-base depositories, such as the Protein Data Bank (PDB).[10] These records provide the three-dimensional structure of the relevant biomacromolecule active site. Further, the progressively increasing development of sophisticated molecular modeling suites allows the researcher to explore and characterize the interactions between a given substrate and the amino acids making up the catalytic site. In this context, the reaction mechanism of α-chymotrypsin was deduced, in part, from its three-dimensional structure determined by X-ray crystallography[11] (Fig. 1). The enzyme contains three subunits, the A, B and C chains,

* Corresponding author. Tel.: +39-040-6763750; fax: +39-040-569823; e-mail: sabrinap@dicamp.units.it

0957-4166/02/$ - see front matter
PII: S0957-4166(02)00144-1

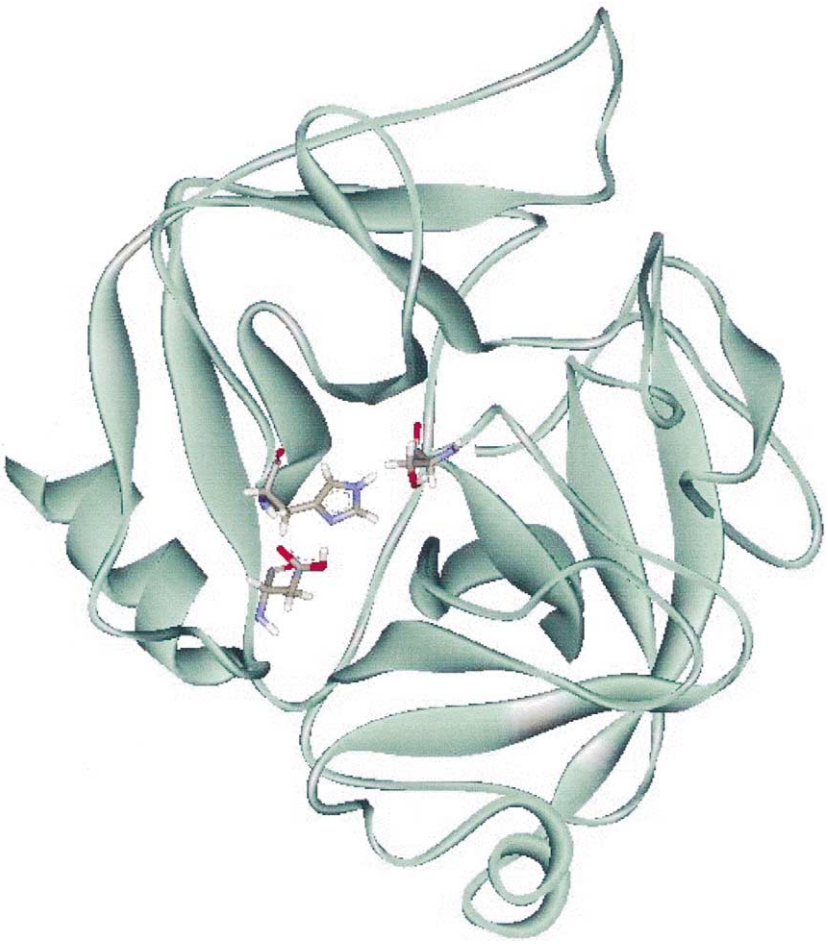

Figure 1. Energy-relaxed model of the three-dimensional structure of α-CT (ribbon model). The catalytic amino acid triad is highlighted in color using a stick style.

which have 13, 1331 and 97 residues, respectively. The quaternary structure of this extracellular protein is stabilized by disulfide bridges between the subunits. The molecule contains a hydrophobic cleft, a crevice in the surface of the protein that is bordered by the side chains of several hydrophobic amino acid residues. This cleft serves as the binding site for specific amino acids on the substrate. Because of its shape, the residues lining the cleft are in the right position to participate in hydrophobic interactions with the large apolar side chains of Phe, Tyr and Trp. The catalytic activity of α-chymotrypsin depends on three amino acid residues: histidine 57, aspartate 102, and serine 195. These amino acids are distant from one another in the primary structure of the protease, but close together in the folded, native conformation (see Fig. 1).

Studies of the SARs in the hydrolysis of ester derivatives of β-aryl-α-amino acids and their analogs by α-chymotrypsin, coupled to X-ray diffraction data and amino acid sequence determination, have led to inferences about the dimensions of the active site, the interactions between enzyme and substrate which affect reactivity and stereoselectivity, and the reactive orientation and conformation of the substrate into the active site. Thus, for this series of compounds, the aryl binding site, *ar*, is situated in a pocket comprising residues 189–194 on one side, and 214–220 on the other; the aromatic group in the binding of formyl L-tryptophane is proposed to be between the peptide bonds of Ser 190-Cys 191, Cys 191-Met 192 and Trp 215-Gly 216. The α-acylamido group has its N–H directed to the C=O of Ser 214, indicated *am*, and its C=O transoid, toward the γ-CH_2 of Met 192; the α-H is directed towards the α-H of Met 192, *h*. Finally, the hydrolyzing group is directed toward the essential –O–H–N of Ser 195 and His 57, *n*.[12,13]

Based on this information, Gillan et al. have studied the hydrolysis of methyl D-pyroglutamates (5-carbomethoxy-2-pyrrolidinones) by α-chymotrypsin, and discussed the results of the enantioselectivity obtained on the basis of different modes of association of the substrate with the active site, and the reactive orientation of the α-acylamido and hydrolyzing groups.[14]

A number of substances based on the γ-lactam (2-pyrrolidinone) structure, besides being key intermediates in the synthesis of many biologically important compounds,[15–17] themselves exhibit interesting biological and pharmacological properties, such as psychotropic, antihypertensive and antimuscarinic activity.[18–20] Nonetheless, despite their intrinsic potentiality for biological activity, both the racemic form and

the enantiomerically pure derivatives of the γ-lactam bearing the carboxylic group at the β-position have received little attention. In a recent paper from our group,[21] a series of racemic methyl esters of 1-alkyl-5-oxo-3-pyrrolidinecarboxylic acids were treated for the first time by enzymatic resolution with several enzymes, such as Pig liver acetone powder (PLAP), Porcine pancreatic lipase (PPL), α-chymotrypsin (α-CT), *Candida rugosa* lipase (CRL) and *Rhizomucor miehei* lipase (MML). Our interest in the enantiomerically pure form of 1-alkyl-5-oxo-3-pyrrolidinecarboxylic acid derivatives stems from the fact that their naturally occurring oxygen analogs (i.e. paraconic acid derivatives) possess interesting biological properties[22] and these aza analogs have the potential to be more effective, due to the lower toxicity of the lactam ring compared to the lactone.[23] In our study, the case of α-chymotrypsin was of particular interest, since our experiments further revealed that, at high conversion values, whilst all the unreacted esters **1a**–**c** were recovered with a fairly good enantiomeric excess (*R*)-(−)-**1a**, e.e. 99%; (*R*)-(+)-**1b**, e.e. 95%; (*R*)-(+)-**1c**, e.e. 99%), in the case of the unsubstituted lactam **1d** no enantiomeric excess was detected (see Fig. 2).

In the light of these findings, we report herein the detailed molecular modeling study related to the hydrolysis of the β-carbomethoxy-γ-lactams **1a**–**d** by α-chymotripsyn, aimed at probing its substrate specificity and explaining its enantioselectivity in terms of its three-dimensional structure and the interaction energy between the ligand and the amino acids forming the protein active site.

2. Calculations

All simulations were run on a Silicon Graphics Origin 200 and performed by using the program packages AutoDock (v. 3.0),[24] AMBER 6.0,[25,26] *Cerius*^{2} (v. 4.2),[27] Discover[28] and in-house developed codes (stand-alone and add-on to the commercial software).

The starting 3-D model of α-chymotrypsin (α-CT) was based on the X-ray crystallographic structure of the α-CT-eglin C complex (PBD code: 1ACB[29]). Water molecules in the coordinate file were removed, and hydrogens were added to the protein backbone and side chains with the PARSE module of the AMBER 6.0 package. All ionizable residues were considered in the standard ionization state at neutral pH. The all-atom force field (FF) parameters by Cornell et al.[30] (in *parm94.dat* file of the AMBER 6.0 code) was applied for protein relaxation. The primary cut-off distance for non-bonded interaction was set to 12 Å, the cut-off taper for the Coulomb and van der Waals interactions were 1.2 and 2, respectively. The GB/SA continuum solvation model[31,32] was used to mimic a water environment. Geometry refinement was carried out using the SANDER module via a combined steepest descent—conjugate gradient algorithm, using as a convergence criterion for the energy gradient the root-mean-square of the Cartesian elements of the gradient equal to 0.01 kcal/(mol Å). As expected, no relevant structural changes were observed between the active site of the α-CT relaxed structure and the original 3-D structure.

The model structures of both enantiomers of the β-carbomethoxy-γ-lactams **1a**–**d** were generated using the 3-D sketcher tool of *Cerius*^{2}. All molecules were subjected to an initial energy minimization using Discover. In this case, the convergence criterion was set to 10^{-4} kcal/(mol Å). The conformational search was carried out using a combined molecular mechanics/molecular dynamics simulated annealing (MDSA) protocol.[33] Accordingly, the relaxed structures were subjected to five repeated temperature cycles (from 298 to 1000 K and back) using constant volume/constant temperature (NVT) MD conditions. At the end of each annealing cycle, the structures were again energy minimized to converge below 10^{-4} kcal/(mol Å), and only the structures corresponding to the minimum energy were used for further modeling. The electrostatic charges for the geometrically optimized lactam molecules were obtained by restrained electrostatic potential fitting,[34] and the electrostatic potentials were produced by single-point quantum mechanical calculations at the Hartree–Fock level with a 6-31G* basis set. All ab initio calculations were carried out with *DMol*^{3},[35] as implemented in the *Cerius*^{2} modeling suite.

To proceed with docking simulation, all non-polar hydrogen atoms of the small organic molecules were deleted, and their charges were automatically added to those of the corresponding carbon atom by the program AutoTors included in the suite AutoDock. The relevant grids of affinity potentials used by AutoDock were calculated by running the program AutoGrid. In order to encase a reasonable region of the protein surface and interior volume, centered on the crystallographic identified binding site, the grids were 60 Å on each side. Grid spacing (0.375 Å), and 120 grid points were applied in each Cartesian direction so as to calculate mass-centered grid maps. Amber 12-6 and 12-10 Lennard–Jones parameters were used in modeling van der Waals interactions and hydrogen bonding (N–H, O–H and S–H), respectively. In the generation of the

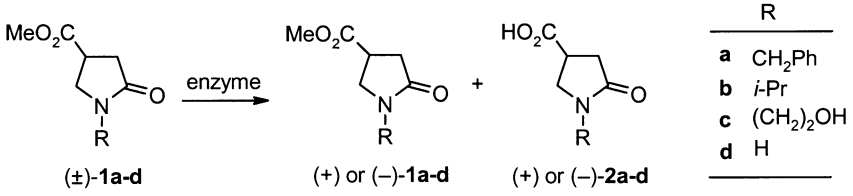

Figure 2. Enzymatic resolution of the β-carbomethoxy-γ-lactams considered by α-CT.

electrostatic grid maps, the distance dependent relative permittivity of Mehler and Solmajer[36] was applied.

For the docking of each cyclic enantiomer to the protein, 300 Monte Carlo/Simulated Annealing (MC/SA) runs were performed, with 100 constant temperature cycles for simulated annealing. Translation, quaternion parameters and torsions were set at random before SA runs. Each cycle had a maximum of 20,000 accepted or rejected moves, the minimal energy structure being passed to the next cycle. The temperature was reduced by a 0.95 factor per cycle from an initial value of RT = 100 cal/mol. For these calculations, the GB/SA implicit water model[31,32] was again used to mimic the solvated environment. The rotation of the angles ϕ and φ, and the angles of side chains were set free during the calculations. All other parameters of the MC/SA algorithm were kept as default. Following the docking procedure, all structures of each lactam enantiomer were subjected to cluster analysis with a tolerance of 1 Å for an all-atom root-mean-square (RMS) deviation from a lower-energy structure representing each cluster family. The structure with the lowest interaction energy was selected for further evaluation.

Each best lactam enantiomer/α-chymotrypsin complex resulting from the automated docking procedure was further refined in the AMBER suite using the quenched molecular dynamics method (QMD). In this case, 100 ps MD simulation at 298 K were employed to sample the conformational space of the lactam–enzyme complex in the GB/SA continuum solvation environment.[31,32] The integration step was equal to 1 fs. After each ps, the system was cooled to 0 K, the structure was extensively minimized, and stored. To prevent global conformational changes of the enzyme, the backbone of the protein binding site were constrained by a harmonic force constant of 100 kcal/Å, whereas the amino acid side chains and the ligands were allowed to move without any constraint.

For the calculation of the binding free energy in water, the best energy configuration of each complex resulting from the previous step was solvated by a cubic box of TIP3P water molecules[37] extended at least 10 Å in each direction from the solute, and an appropriate number of counter ions were added to neutralize the system. The periodic boundary conditions with constant pressure of 1 atm were applied, and long-range non-bonded van der Waals interactions were truncated by using a 8 Å residue-based cut-off. The particle mesh Ewald method[38] was used to treat the long-range electrostatics. Unfavorable interactions within the structures were relieved with steepest descent followed by conjugate gradient energy minimization until the RMS of the elements in the gradient vector was less than 10^{-4} kcal/(mol Å). Each system was gradually heated to 298 K in three intervals, allowing a 5 ps interval per each 100 K, and then equilibrated for 25 ps at 298 K, followed by 400 ps of data collection runs. The SHAKE algorithm was applied to constrain all bonds to their equilibrium values, thus removing high frequency vibrations.[39] An integration time step of 2 fs was used with constant temperature, being the temperature maintained at a constant value by the Berendsen coupling algorithm,[40] with separate solute–solvent and solvent–solvent coupling. A total of 400 snapshots were saved during data collection period, one snapshot per 1 ps of MD simulation.

The binding free energy ΔG_{bind} of each complex in water was calculated according to the procedure proposed by Srinivasan et al.,[41] and will be briefly described below. According to this method, ΔG_{bind} is calculated as:

$$\Delta G_{\text{bind}} = \Delta G_{\text{MM}} + \Delta G^{\text{C}}_{\text{sol}} - \Delta G^{\text{L}}_{\text{sol}} - \Delta G^{\text{P}}_{\text{sol}} - T\Delta S \qquad (1)$$

where ΔG_{MM} is the interaction energy between the ligand and the protein, $\Delta G^{\text{C}}{}_{\text{sol}}$, $\Delta G^{\text{L}}{}_{\text{sol}}$ and $\Delta G^{\text{P}}{}_{\text{sol}}$ are the solvation free energy for the complex, the ligand and the protein, respectively, and $-T\Delta S$ is the conformational entropy contribution to the binding. All energetic analysis was carried out for only a single MD trajectory of the lactam/protein complex considered, with unbound protease and lactam snapshots taken from the snapshots of that trajectory.

ΔG_{MM} can be obtained from the molecular mechanics (MM) interaction energies as:

$$\Delta G_{\text{MM}} = \Delta G^{\text{ele}}_{\text{int}} + \Delta G^{\text{vdW}}_{\text{int}} \qquad (2)$$

where $\Delta G^{\text{ele}}{}_{\text{int}}$ and $\Delta G^{\text{vdW}}{}_{\text{int}}$ are the electrostatic and van der Waals contributions to the interaction energy between the ligand and the receptor. We must point out here that the molecular mechanics energy ΔG_{MM} in Eq. (2) also effectively consists of a valence part, $\Delta G^{\text{val}}{}_{\text{int}}$, but, since the structure of the protein in its bound and unbound state is the same, the contribution of this term to the binding free energy is zero. Accordingly, it term has been omitted in Eq. (2). In our case, these quantities were calculated with the *anal* and *carnal* modules from the AMBER 6.0 suite. The infinite cutoffs for all interactions and the *parm94* force field parameters[30] were applied. The total solvation energy, ΔG_{sol}, is divided in two parts: the electrostatic contribution, $\Delta G^{\text{ele}}{}_{\text{sol}}$, and the non-polar term, $\Delta G^{\text{np}}{}_{\text{sol}}$:

$$\Delta G_{\text{sol}} = \Delta G^{\text{ele}}_{\text{sol}} + \Delta G^{\text{np}}_{\text{sol}} \qquad (3)$$

The polar component of ΔG_{sol} was evaluated with the PB approach.[42] This procedure involves using a continuum solvent model, which represents the solute as a low dielectric medium (i.e. of dielectric constant $\varepsilon = 1$) with embedded charges and the solvent as a high dielectric medium ($\varepsilon = 80$) with no salt. All atomic charges were taken from the Cornell et al. force field,[30] since these are consistent with the MM energy calculations. However, as suggested by Chong et al.,[43] the atomic radii were taken from the PARSE parameter set[44] instead of the *parm94* FF set because of the small size of hydrogens in the latter. The dielectric boundary is the contact surface between the radii of the solute and the radius (1.4 Å) of a water molecule. The numerical solution of the linearized Poisson–Boltzmann equations were solved on a cubic lattice by using the iterative finite-difference method implemented in the

DelPhi software package.[45] The grid size used was 0.5 Å. Potentials at the boundaries of the finite-difference lattice were set to the sum of the Debye–Hückel potentials.

The non-polar contribution to the solvation energy ΔG^{np}_{sol} was calculated from the following equation:[44]

$$\Delta G^{np}_{so} = \gamma SA + b \quad (4)$$

in which $\gamma = 0.00542$ kcal/Å^2, $b = 0.92$ kcal/mol, and SA is the solvent-accessible surface estimated with the MSMS[46] program.

To complete the estimate of the free energy of binding, we should also calculate the entropy components arising from the solute degrees of freedom. Given that our goal is a qualitative comparison of ΔG_{bind} for the different enantiomeric molecules, we assume that the entropies are similar in magnitude for the close-structured lactams. This assumption seems reasonable, given Kuhn and Kollman's calculated values of $T\Delta S$ for various ligands binding to avidin.[47] Also, the results of these two authors show that this term tends to be larger in magnitude the larger the ligand. Since the van der Waals surface areas for all the lactam enantiomers considered in our work—estimated using a modified version of the so-called Connolly dot surfaces algorithm,[48,49] based on semi empirical molecular orbital calculations[50]—is confined within the range of about 39 Å^2 (i.e. from an average value of 244 Å^2 for the (±)-**1a** to an average value of 198 Å^2 for (±)-**1c**), we concluded that the assumption of Kuhn and Kollman could be safely applied to our calculations.

3. Results and discussion

3.1. Methyl 1-(phenylmethyl)-5-oxo-3-pyrrolidinecarboxylate (±)-1a

The experimental results obtained from the enzymatic hydrolysis of the enantiomeric lactams (±)-**1a** indicate that both the unreacted ester (*R*)-(−)-**1a** and the acid (*S*)-(+)-**2a** were recovered with a very high enantiomeric excess, that is e.e. 99% (54% conversion) and 99% (29% conversion), respectively.[21] The corresponding molecular modeling results are consistent with the experimental findings.

Unsurprisingly, computational docking of stereoisomers (±)-**1a**–**d** provides a challenge in terms of the specificity of the protocol used and the ability of the energy evaluation to distinguish between correct and incorrect orientations of the bound substrate. Our previous results in fine-tuning AutoDock procedures for the binding of ligands to different protein receptors[51,52] indicate that the cluster of similar conformations with the lowest energy docked structure always reproduced very closely the crystallographic binding mode.

While interaction with a receptor will certainly perturb the conformational energy of a flexible ligand, high affinity would suggest that the ligand is not highly distorted upon binding. In this particular case, the docking study shows that both stereoisomers (±)-**1a** bind effectively in the selected protein region, with no noticeable energy penalty. In fact, the differences in conformational energy between bound and unbound state of both lactams (±)-**1a** were less 2 kcal/mol (1.40 kcal/mol for (*S*)-**1a** and 1.58 kcal/mol for (*R*)-**1a**, respectively). Following the analysis of the representative clusters (data not shown), the structure believed to represent a significant binding mode in the α-CT binding site were selected for further optimization, according to the QMD procedure described in the previous section.

Fig. 3(a) and (b) shows the resulting molecular models of the docked α-CT/(*S*)-**1a** and α-CT/(*R*)-**1a** complexes, respectively. In the optimized model for (*S*)-**1a**, the lactam fills the entire aryl binding site *ar* (a pocket with residues 189–194 on one side, and 214–220 on the other), from Ser 195 downward a distance of roughly 11 Å. Further, the hydrolyzing $COOCH_3$ group assumes an orientation in space, which could be favorable for the interaction with the catalytic triad His 57, Asp 102 and Ser 195. On the contrary, it is impossible for the other enantiomer (*R*)-**1a** to achieve a similar spatial arrangement into the enzyme active site, because of the different orientation of the benzyl group. Any attempt to eliminate this unfavorable situation in (*R*)-**1a** by rotation of the aromatic ring causes it to penetrate the enzyme backbone, and is thus discarded.

As expected, the evolution of the dynamics was consistent with a stabilized system with minimal fluctuations in total energy being exhibited as a function of time. Indeed, molecular dynamics snapshots of the conformation of each α-CT/lactam complex as a function of time revealed a distribution of peptide conformation virtually indistinguishable from that shown in Fig. 3. In order to examine the individual contribution of the protein residues to the non-bonding components of the interaction energy ΔE^{nb}_{tot}, the collected frames were further processed, and the interaction energy between each lactam and the binding site were decomposed on a residue basis using the *anal* module of AMBER for the most favorable binding obtained for each lactam. The corresponding values obtained for the enantiomers (*S*)/(*R*)-**1a** are collected in Table 1. We must emphasize that these energies serve to qualitatively describe the binding characteristics and are not equivalent to free energies of binding (vide infra), as desolvation contributions are not included.

The analysis of the trajectories of the dynamics simulations for the α-CT/(*S*)-**1a** complex indicates that there is a constant presence of a H-bond between the oxygen atom of the OCH_3 group of (*S*)-**1a** which involves the OH group of Ser 195, and, alternatively, the NH of the peptide bond between Ser 195 and Asp 194. The average dynamic lengths (ADL) of these two H-bonds are 2.20 and 2.94 Å, respectively. Further, in this situation the catalytic couple His 57–Asp 102 presents a stable H-bond, of average dynamic length equal to 2.47 Å.

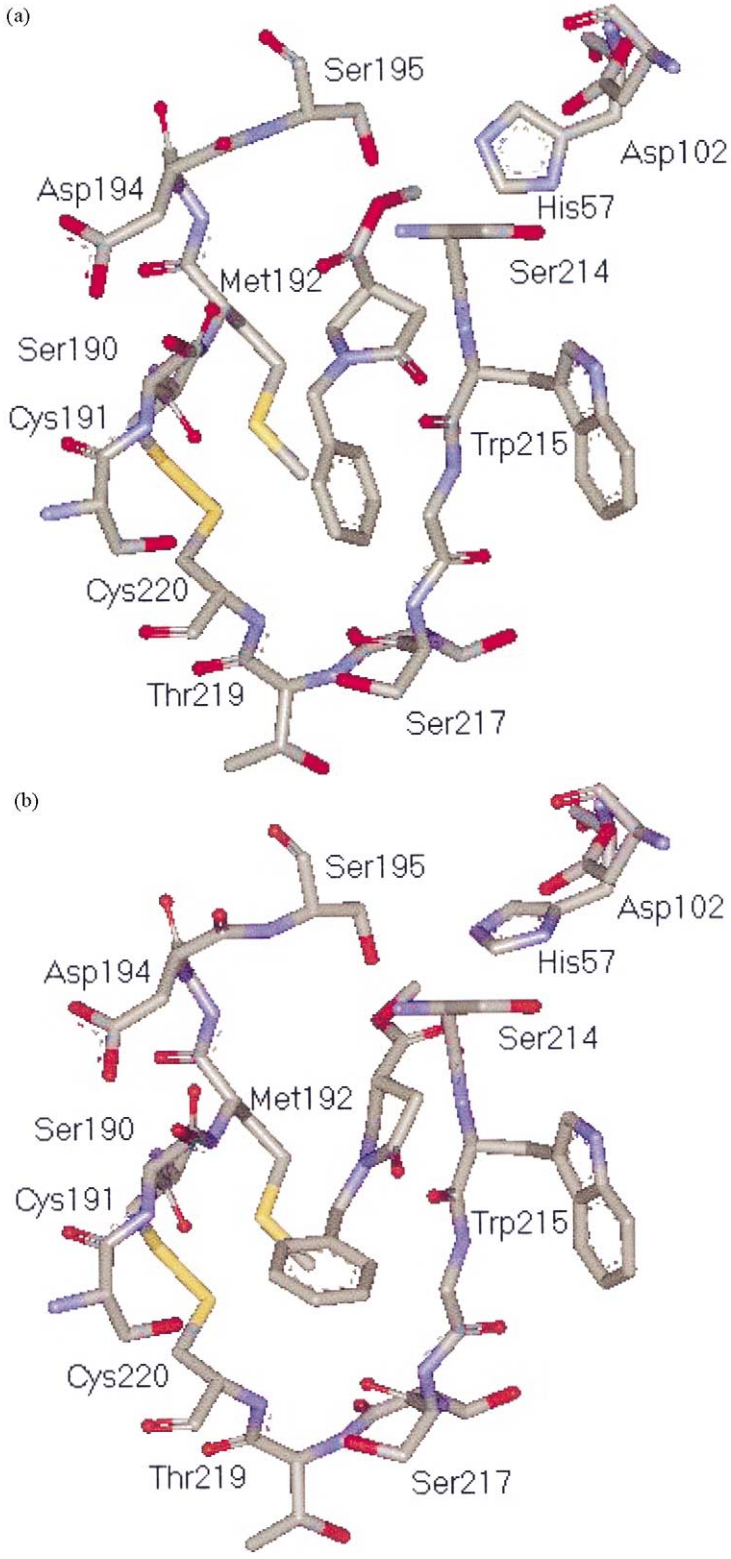

Figure 3. Optimized molecular model of the docked α-CT/(*S*)-**1a** (a) and α-CT/(*R*)-**1a** (b) complexes. For the sake of simplicity, only the amino acids forming the catalytic triad (His 57, Asp 102, and Ser 195), as well as those pertaining to the binding site are shown. Hydrogen atoms are also omitted for clarity.

For the alternative complex α-CT-(*R*)-**1a**, whilst the H-bond between the OCH_3 group of the ligand and the hydroxyl group of Ser 195 is still present (ADL = 2.63 Å), the other, alternative intermolecular interactions described above may form intermittently throughout the MD simulation, but it does not persist during the entire trajectory. This accounts for the enhanced values of $\Delta E^{nb}{}_{tot}$ for His 57, Asp 102, and Asp 104 in the case of (*S*)-**1a**, as well as for the small difference in interaction energy between the two isomers and Ser 195

Table 1. Residue-based decomposition of the non-bonding interaction energies $\Delta E^{nb}{}_{tot}$ (kcal/mol) between the lactam enantiomers (*S*)/(*R*)-**1a** and the α-CT binding site in the orientations bound studied

Residue	(*S*)-**1a** $\Delta E^{nb}{}_{vdW}$	(*S*)-**1a** $\Delta E^{nb}{}_{coul}$	(*S*)-**1a** $\Delta E^{nb}{}_{tot}$	(*R*)-**1a** $\Delta E^{nb}{}_{vdW}$	(*R*)-**1a** $\Delta E^{nb}{}_{coul}$	(*R*)-**1a** $\Delta E^{nb}{}_{tot}$
His 57	−2.6	−2.0	−4.6	−1.8	−0.2	−2.0
Asp 102	−4.9	−2.5	−7.4	−2.4	−1.4	−3.8
Ser 189	−1.7	−0.6	−2.3	−1.5	−0.5	−2.0
Ser 190	−1.3	−0.2	−1.5	−1.2	−0.1	−1.3
Cys 191	−3.6	−0.2	−3.8	−2.1	−0.1	−2.2
Met 192	−4.0	−0.3	−4.3	−2.0	−0.1	−2.1
Gly 193	−0.4	−0.0	−0.4	−0.4	−0.0	−0.4
Asp 194	−5.5	−3.2	−8.7	−2.6	−1.9	−4.5
Ser 195	−4.8	−3.0	−7.8	−4.5	−3.0	−7.5
Ser 214	−3.9	−2.7	−6.6	−1.5	−0.7	−2.2
Trp 215	−5.3	−1.7	−7.0	−2.2	0.9	−3.1
Gly 216	−1.0	−1.2	−2.2	−0.9	−0.1	−1.0
Ser 217	−2.0	−0.8	−2.8	−1.7	−0.4	−2.1
Ser 218	−1.4	−0.7	−2.1	−0.9	−0.8	−1.7
Thr 219	−1.8	−0.3	−2.1	−1.6	−0.1	−1.7
Cys 220	**−3.3**	**−0.3**	**−3.6**	**−2.0**	**−0.0**	**−2.0**

reported in Table 1. During the course of the MD experiments, a further intermolecular interaction of the H-bond type is evidenced between the carbonyl oxygen of the (*S*)-**1a** lactam ring and the NH of the peptidic bond between Ser 214 and Trp 215, characterized by an ADL of 3.0 Å. The same stabilization cannot be achieved in the case of (*R*)-**1a**, and this is accounted for by the relevant values of $\Delta E^{nb}{}_{tot}$ for these two amino acids and the corresponding lactam enantiomers (see Table 1).

Finally, the more favorable insertion mode of the benzyl group of (*S*)-**1a** into the aryl binding site *ar* of the α-CT helps in maximizing interactions between protein and ligand. Indeed, the N atom of the peptide bond between Trp 215 and Gly 216 appears to form a dipole–quadrupole interaction with the phenyl group of the (*S*)-**1** lactam (it comes as close as 3.5 Å to the aryl lactam substituent); further, this arrangement give rise to slightly more favorable van der Waals dispersions with both the hydrophobic side chain of Met 192 and the disulfide bridge between Cys 191 and Cys 220 (see Fig. 3 and Table 1). Lastly, π-interaction between the aromatic ring of Trp 215 of α-CT and the benzyl moiety of the (*S*)-**1a** substrate may have a substantial role in further stabilizing the relevant complex.

The estimated free energy of binding for the two complexes of (*S*)- and (*R*)-**1a** lactam and α-CT, obtained from the procedure detailed in the previous section, are reported in Table 2. From these results it is obvious that the (*S*)-**1a** enantiomer binds more tightly to α-CT. This molecule not only has the most favorable van der Waals interaction with the protein ($\Delta\Delta G^{vdW}{}_{int}$ (*S*–*R*) = –0.9 kcal/mol), but also the most favorable total electrostatic contribution ($\Delta\Delta G^{ele}{}_{tot}$ (*S*–*R*) = −1.9 kcal/mol). It is very important to consider the electrostatic component of the molecular mechanics energy $\Delta G^{ele}{}_{int}$ together with the electrostatic contribution to solvation $\Delta G^{ele}{}_{sol}$ when examining the role of electrostatics in any protein/ligand complex formation. In fact, as proven by several studies,[53–59] electrostatics generally disfavor the docking of a ligand/receptor couple because the unfavorable change in the electrostatic of solvation is mostly, but not fully, compensated by the favorable electrostatics within the resulting host–guest complex. Indeed, the total electrostatic energy contributions $\Delta G^{ele}{}_{tot}$ to the binding free energy for both the (*S*)- and (*R*)-**1a**/α-CT complexes are not favorable, with values of 1.8 and 3.7 kcal/mol, respectively. Hence, the (*S*)-**1a**/α-CT complex formation is less unfavorable than the corresponding, opposite enantiomer complex because of a less positive, total electrostatic term, in which the penalty paid by the electrostatic of solvation is better compensated by favorable electrostatic interaction within the complex. This calculation suggests than that a crucial factor for the enantioselective hydrolysis of these γ-lactams by α-CT is to achieve an optimal electrostatic interaction between the ligand and the protein active site but also to suffer less desolvation penalty. Thus, even though electrostatics overall tend to destabilize both (*S*)- and (*R*)-**1a** complex formation, it is the optimized balance of opposing electrostatic contributions and a more favorable dispersion term that leads to tighter binding of the (*S*)-**1a** enantiomers to α-CT.

Finally, it is worth noticing here that the binding free energy values between (*S*)/(*R*)-**1a** and α-CT calculated

Table 2. Energy terms and binding free energies[a] (kcal/mol) for the lactam enantiomers (*S*)/(*R*)-**1a** with α-CT

	(*S*)-**1a**	(*R*)-**1a**
$\Delta G^{vdW}{}_{int}$	−9.1 ± 0.1	−8.2 ± 0.1
$\Delta G^{ele}{}_{intl}$	−94.5 ± 0.3	−93.5 ± 0.4
ΔG_{MM}	−103.6	−101.7
$\Delta G^{np}{}_{sol}$	−3.2 ± 0.0	−3.0 ± 0.0
$\Delta G^{ele}{}_{sol}$	99.5 ± 0.2	100.2 ± 0.2
ΔG_{sol}	96.3 ± 0.2	97.2 ± 0.2
$\Delta E^{ele}{}_{tot}$	1.8	3.7
ΔG_{bind}	−7.3	−4.5

[a] $T\Delta S$ not included (see text).

Table 3. Residue-based decomposition of the non-bonding interaction energies $\Delta E^{nb}{}_{tot}$ (kcal/mol) between the lactam enantiomers (*S*)/(*R*)-**1b** and the α-CT binding site in the bound orientations studied

Residue	(*S*)-**1b** $\Delta E^{nb}{}_{vdW}$	(*S*)-**1b** $\Delta E^{nb}{}_{coul}$	(*S*)-**1b** $\Delta E^{nb}{}_{tot}$	(*R*)-**1b** $\Delta E^{nb}{}_{vdW}$	(*R*)-**1b** $\Delta E^{nb}{}_{coul}$	(*R*)-**1b** $\Delta E^{nb}{}_{tot}$
His 57	−2.9	−2.9	−5.8	−2.8	−2.8	−5.6
Asp 102	−5.0	−2.8	−7.8	−4.8	−2.4	−7.2
Ser 189	−1.6	−0.5	−2.1	−1.4	−0.4	−1.8
Ser 190	−1.2	−0.1	−1.3	−1.1	−0.1	−1.2
Cys 191	−0.9	−0.2	−1.1	−0.8	−0.2	−1.0
Met 192	−4.4	−1.6	−6.0	−2.8	−1.2	−4.0
Gly 193	−1.5	−1.8	−3.2	−0.2	−0.1	−0.3
Asp 194	−5.7	−3.4	−9.1	−2.2	−1.5	−3.7
Ser 195	−4.4	−3.1	−7.5	−4.3	−2.9	−7.2
Ser 214	−1.5	−0.3	−1.8	−1.3	−0.4	−1.7
Trp 215	−0.9	−0.5	−1.4	−0.8	−0.4	−1.2
Gly 216	−0.2	−0.0	−0.2	−0.2	−0.0	−0.2
Ser 217	−1.9	−0.7	−2.6	−1.5	−0.5	−2.0
Ser 218	−1.3	−0.5	−1.8	−1.1	−0.7	−1.8
Thr 219	−1.8	−0.3	−2.1	−1.4	−0.1	−1.5
Cys 220	−0.8	−0.2	−1.0	−0.7	−0.0	−0.7

with our procedure (as well as for all other series of compounds considered, vide infra) are in the same range of the values obtained experimentally by several authors for different drugs[60,61] (i.e. –4.0 to –7.0 kcal/mol), notwithstanding the approximation of the adopted methodology and the cancellation of large numbers required.

3.2. Methyl 1-(methylethyl)-5-oxo-3-pyrrolidinecarboxylate (±)-1b

The experimental evidence[21] about the enantioselective hydrolysis of the (±)-**1b** lactams by α-CT shows that, although to a slightly lesser extent with respect to the (±)-**1a** lactams, again both the unreacted ester (*R*)-(−)-**1b** and the acid (*S*)-(+)-**2b** were recovered with high enantiomeric excess, that is e.e. 95% (65% conversion) and 88% (21% conversion), respectively.

As in the previous case, the automated docking procedure was able to place both enntiomers of (±)-**1b** in the protease active site without marked conformational strain (the difference in conformational energy of the lactams in the bound and unbound state being 1.60 kcal/mol for the (*S*)-**1b** and 1.92 kcal/mol for (*R*)-**1b**), respectively. Fig. 4(a) and (b) shows the resulting molecular models of the docked α-CT/(*S*)-**1b** and α-CT/(*R*)-**1b** complexes, respectively, after further QMD refinement, whereas the protein residue-based contribution to the non-bonding components of the interaction energy are reported in Table 3.

Inspection of the docked (*S*)/(*R*)-**1b** in the α-CT enzyme reveals that the methyl carboxylate group of both lactams is located in a favorable position with respect to the catalytic triad His 57, Asp 102 and Ser 195, which, in both cases, present a stable H-bond pattern between the NE2 atom of His 57 and the OH group of Ser 195 (ADL = 2.17 Å), and between the carboxylate oxygen OD1 of Asp 102 and the NH of the peptide bond of Ala 56 and His 57 (ADL = 2.22 Å). Nonetheless, for (*S*)-**1b**, an analysis of the corresponding MD trajectory indicates that the C=O group of the ester accepts a hydrogen bond from the NH of the peptide bond between Asp 194 and Ser 195 (ADL = 1.98 Å). Further, the same group is involved in another, alternative but persistent H-bond with the NH of the peptide bond between Met 192 and Gly 193, characterized by an average dynamic length of 2.24 Å. Such interactions are not detected in the dynamic trajectory of the corresponding, opposite enantiomer (*R*)-**1b**, and this is properly accounted for by the relevant energy values listed in Table 3. The aliphatic, ramified chain substituent at the lactam ring N atom is positioned within the aryl binding site, *ar*, where it favorably interacts with the hydrophobic side chain of Met 192. For (*S*)-**1b**, during the simulation the two chains contact each other at a C–C– average distance of about 4 Å, thereby increasing mutually their hydrophobic contact area and hence stabilizing the complex. A similar situation is encountered for the other enantiomers, although the slightly greater distance between the two chains (about 5 Å) make this interaction weaker (see Table 3).

Table 4 shows all energy terms and the binding free energy for the α-CT complexes with the two enantiomers (*S*)/(*R*)-**1b**. Our estimates reveal that, as in the

Table 4. Energy terms and binding free energies[a] (kcal/mol) for the lactam enantiomers (*S*)/(*R*)-**1b** with α-CT

	(*S*)-**1b**	(*R*)-**1b**
$\Delta G^{vdW}{}_{int}$	−11.1 ± 0.1	−10.5 ± 0.1
$\Delta G^{ele}{}_{intl}$	−77.5 ± 0.2	−76.7 ± 0.2
ΔG_{MM}	−88.6	−87.2
$\Delta G^{np}{}_{sol}$	−2.6 ± 0.0	−2.4 ± 0.0
$\Delta G^{ele}{}_{sol}$	84.7 ± 0.1	85.3 ± 0.2
ΔG_{sol}	82.1 ± 0.1	82.9 ± 0.2
$\Delta G^{ele}{}_{tot}$	4.6	6.2
ΔG_{bind}	−6.5	−4.3

[a] $T\Delta S$ not included (see text).

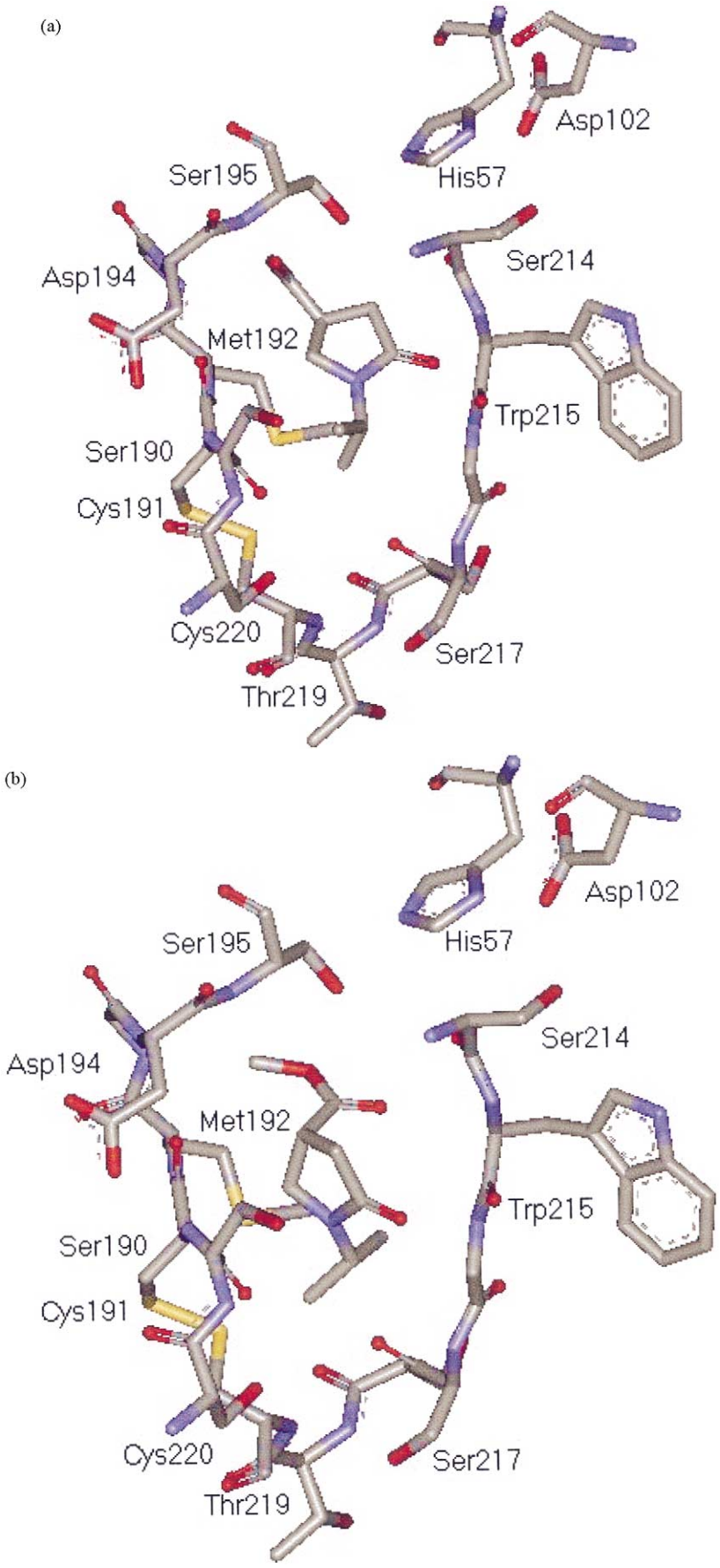

Figure 4. Optimized molecular model of the docked α-CT/(*S*)-**1b** (a) and α-CT/(*R*)-**1b** (b) complexes. For the sake of simplicity, only the amino acids forming the catalytic triad (His 57, Asp 102, and Ser 195), as well as those pertaining to the binding site are shown. Hydrogen atoms are also omitted for clarity.

Table 5. Residue-based decomposition of the non-bonding interaction energies $\Delta E^{nb}{}_{tot}$ (kcal/mol) between the lactam enantiomers (*S*)/(*R*)-**1c** and the α-CT binding site in the bound orientations studied

Residue	(*S*)-**1c** $\Delta E^{nb}{}_{vdW}$	(*S*)-**1c** $\Delta E^{nb}{}_{coul}$	(*S*)-**1c** $\Delta E^{nb}{}_{tot}$	(*R*)-**1c** $\Delta E^{nb}{}_{vdW}$	(*R*)-**1c** $\Delta E^{nb}{}_{coul}$	(*R*)-**1c** $\Delta E^{nb}{}_{tot}$
His 57	−3.0	−2.8	−5.8	−2.8	−2.9	−5.7
Asp 102	−5.2	−2.9	−8.1	−4.9	−2.2	−7.1
Ser 189	−4.6	−3.5	−8.1	−1.2	−0.3	−1.5
Ser 190	−4.2	−3.1	−7.3	−1.1	−0.3	−1.4
Cys 191	−0.8	−0.1	−0.9	−0.8	−0.2	−1.0
Met 192	−2.0	−1.0	−3.0	−4.8	−1.2	−6.0
Gly 193	−0.5	−0.2	−0.7	−1.3	−1.1	−2.4
Asp 194	−5.5	−3.1	−8.6	−2.0	−1.1	−3.3
Ser 195	−5.2	−3.6	−8.8	−4.1	−2.5	−6.6
Ser 214	−1.4	−0.3	−1.7	−1.2	−0.4	−1.6
Trp 215	−0.7	−0.5	−1.2	−1.8	−1.4	−3.2
Gly 216	−0.2	−0.1	−0.3	−1.2	−1.1	−2.3
Ser 217	−1.7	−0.7	−2.4	−1.5	−0.3	−1.8
Ser 218	−1.5	−0.7	−2.2	−1.2	−0.8	−2.0
Thr 219	−1.2	−0.3	−1.5	−1.2	−0.1	−1.3
Cys 220	−0.7	−0.2	−0.9	−0.7	−0.1	−0.8

case of the previous enantiomeric couple, the energy balance favors binding of (*S*)-**1b**. Again, for both lactams the effective formations of these complexes are driven by the molecular mechanics interaction energy components and the non-polar contribution to solvation; as expected, these energetic terms are very similar for both enantiomers. The total electrostatic contributions for both complex formations are again unfavorable, being equal to 4.6 and 6.2 kcal/mol, respectively, but the net energetic result is favored by the positive balance between opposing electrostatic terms.

3.3. Methyl 1-(2-hydroxyethyl)-5-oxo-3-pyrrolidinecarboxylate (±)-1c

The experimental enzymatic hydrolysis by α-CT of the third couple of enantiomeric β-carbomethoxy-γ-lactams considered, i.e. (±)-**1c**, confirmed the enantioselectivity of these protease towards these types of prodrugs, although, in this case, the unreacted ester (*R*)-**1c** was recovered with high enantiomeric excess (e.e. 99% at 54% conversion), while the corresponding acid (*S*)-**2c** was obtained with a moderate enantiomeric excess (e.e. 31% at 39% conversion).[21]

The results obtained from the application of the molecular docking procedure and their further refinements described above are graphically depicted in Fig. 5(a) and (b). As we may see from Fig. 5, both lactams can be easily docked into the protein active site without a noticeable energy penalty. Indeed, the corresponding conformational energy difference between bound and unbound states for the lactam molecules is small (1.10 and 1.20 kcal/mol for (*S*)-**1c** and (*R*)-**1c**, respectively). Nonetheless, the (*S*)-**1c** ester is not only more deeply embedded into the α-CT binding site (8.4 Å down from Ser 215 versus 6.4 Å for (*R*)-**1c**), but also the hydrolyzing methyl ester group is located in a more favorable position for interaction with the catalytically-active amino acids. Indeed, although the H-bond network involving the catalytic triad is still present in both cases, the (*S*)-**1c** enantiomer appears to have its oxygen atom of the OCH_3 residue hydrogen bonded to the OH group of Ser 195 (ADL = 1.99 Å). The analysis of the corresponding MD trajectory also reveals that the same atom is involved in another, alternative H-bond with the NH group of the peptidic bond between Asp 194 and Ser 195, characterized by an average dynamic length of 2.48 Å. Also, the carbonyl group of the ester is involved in this type of intermolecular interaction with the OH group of Ser 195 (ADL = 2.45 Å). In the case of the opposite enantiomer, due to the different orientation of the molecule within the α-CT active site, the oxygen atom of the OCH_3 group is stably H-bonded to the HN group of the peptide bond between Met 192 and Gly 193 (ADL = 1.97 Å), which alternatively interacts also with the C=O group (ADL = 2.11 Å). Finally, the hydroxyl substituent group of both lactams forms a persistent H-bond with the NH group of the peptide bond between Ser 189 and Ser 190 in the case of the (*S*)-**1c** enantiomer (ADL = 2.46 Å), and with the NH group of the peptide bond between Trp 215 and Gly 216 in the case of (*R*)-**1c** (ADL = 2.44 Å). These intermolecular interactions are accounted for by the corresponding values of the residue-based energy decomposition of the non-bonding interaction energies $\Delta E^{nb}{}_{tot}$ reported in Table 5.

Table 6. Energy terms and binding free energies[a] (kcal/mol) for the lactam enantiomers (*S*)/(*R*)-**1c** with α-CT

	(*S*)-**1c**	(*R*)-**1c**
$\Delta G^{vdW}{}_{int}$	−10.5 ± 0.1	−9.8 ± 0.1
$\Delta G^{ele}{}_{intl}$	−82.1 ± 0.3	−81.4 ± 0.2
ΔG_{MM}	−92.6	−91.2
$\Delta G^{np}{}_{sol}$	−2.4 ± 0.0	−2.1 ± 0.0
$\Delta G^{ele}{}_{sol}$	86.3 ± 0.2	86.5 ± 0.1
ΔG_{sol}	83.9 ± 0.2	84.4 ± 0.1
$\Delta G^{ele}{}_{tot}$	1.8	3.0
ΔG_{bind}	−6.3	−4.7

[a] $T\Delta S$ not included (see text).

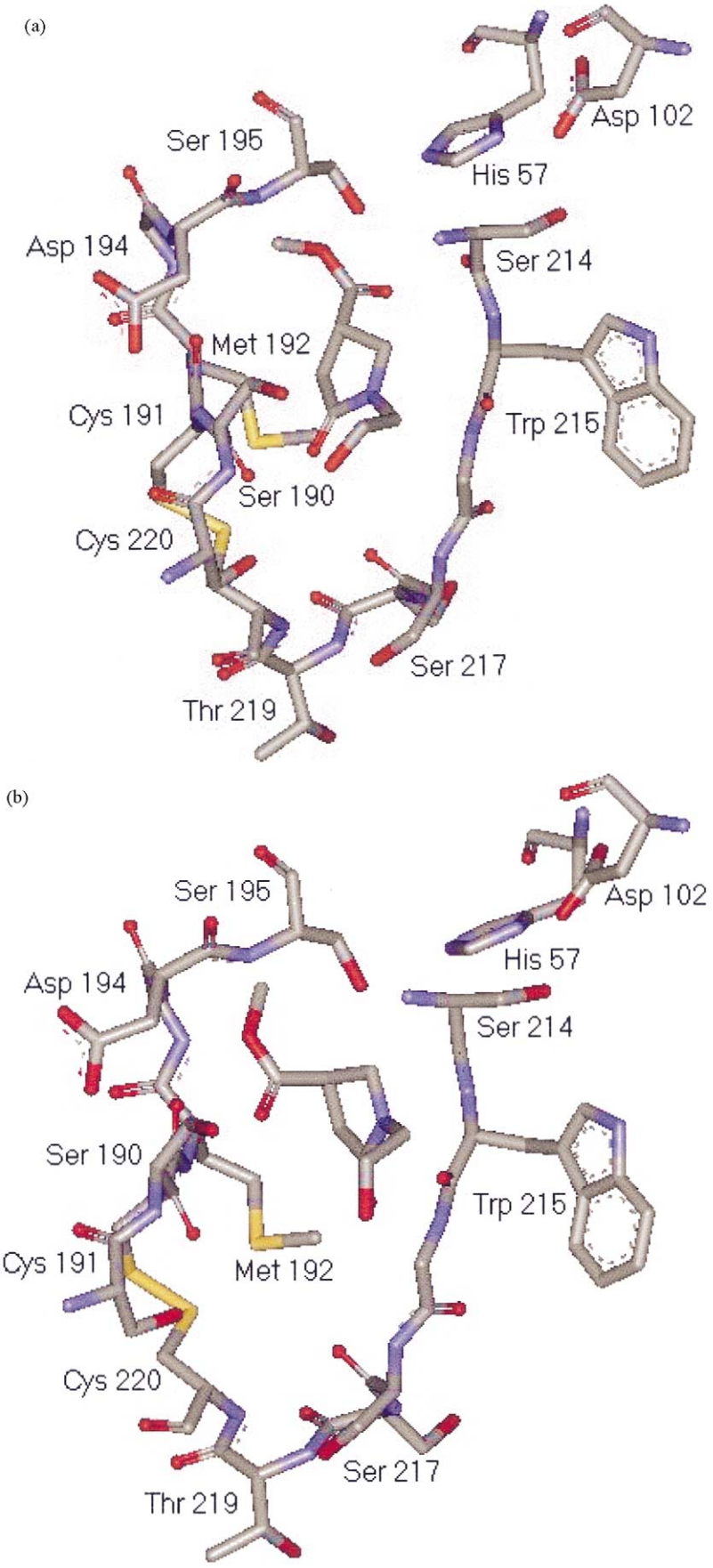

Figure 5. Optimized molecular model of the docked α-CT/(*S*)-**1c** (a) and α-CT/(*R*)-**1c** (b) complexes. For the sake of simplicity, only the amino acids forming the catalytic triad (His 57, Asp 102, and Ser 195), as well as those pertaining to the binding site are shown. Hydrogen atoms are also omitted for clarity.

Table 7. Residue-based decomposition of the non-bonding interaction energies $\Delta E^{nb}{}_{tot}$ (kcal/mol) between the lactam enantiomers (*S*)/(*R*)-**1d** and the α-CT binding site in the bound orientations studied

Residue	(*S*)-**1d** $\Delta E^{nb}{}_{vdW}$	(*S*)-**1d** $\Delta E^{nb}{}_{coul}$	(*S*)-**1d** $\Delta E^{nb}{}_{tot}$	(*R*)-**1d** $\Delta E^{nb}{}_{vdW}$	(*R*)-**1d** $\Delta E^{nb}{}_{coul}$	(*R*)-**1d** $\Delta E^{nb}{}_{tot}$
His 57	−3.1	−2.8	−5.9	−2.8	−2.8	−5.6
Asp 102	−5.0	−2.9	−7.9	−4.9	−2.2	−7.1
Ser 189	−1.7	−0.6	−2.3	−1.5	−0.5	−2.0
Ser 190	−4.8	−3.5	−8.3	−4.4	−3.3	−7.7
Cys 191	−1.0	−0.1	−1.1	−0.8	−0.3	−1.1
Met 192	−1.9	−0.3	−2.2	−4.2	−0.5	−4.5
Gly 193	−0.4	−0.3	−0.7	−1.5	−1.2	−2.7
Asp 194	−5.4	−3.4	−8.8	−5.2	−3.1	−8.3
Ser 195	−5.2	−3.6	−8.8	−5.1	−3.5	−8.4
Ser 214	−4.4	−3.3	−7.7	−1.2	−0.4	−1.6
Trp 215	−0.5	−0.3	−0.8	−0.4	−0.4	−0.8
Gly 216	−0.2	−0.1	−0.3	−0.2	−0.1	−0.3
Ser 217	−1.4	−0.8	−2.2	−1.5	−0.2	−1.7
Ser 218	−1.4	−0.7	−2.1	−1.2	−0.7	−1.9
Thr 219	−1.2	−0.3	−1.5	−1.2	−0.1	−1.3
Cys 220	−0.5	−0.2	−0.7	−0.7	−0.0	−0.7

In Table 6 we present the total free energy of binding and its components estimated for the (*S*)/(*R*)-**1c**/αCT complexes. Table 6 clearly shows how the (*S*)-**1c** enantiomer still presents the most favorable value for a tighter binding to α-CT. Again, the favorable input to ΔG_{bind} for these compounds comes from the gain in van der Waals interactions ($\Delta\Delta G^{vdW}{}_{int}$ (*S*–*R*) = −0.7 kcal/mol)), and the nonpolar contributions to solvation ($\Delta\Delta G^{np}{}_{sol}$ (*S*–*R*) = −0.3 kcal/mol). The total electrostatic contributions for both enantiomers are still unfavorable, as expected, being equal to 1.8 kcal/mol for the (*S*)-**1c** and 3.0 kcal/mol for the (*R*)-**1c** enantiomer, respectively. Nonetheless, if compared with the previous two cases, we observed that the values of $\Delta G^{ele}{}_{tot}$ are rather similar for the two enantiomeric lactams (±)-**1a** and (±)-**1c**, whereas this parameter is somewhat higher for the (±)-**1b** couple. Thus, we can speculate that either the contribution of π- and dipole–quadrupole interactions in the case of (±)-**1a**, and the enhanced number of H-bonds present in the case of (±)-**1c**, actually seem to partially compensate for the penalty paid in the electrostatic of solvation upon complex formation for these two series of enantiomers.

3.4. Methyl 5-oxo-3-pyrrolidinecarboxylate (±)-1d

The enzymatic hydrolysis of the last couple of enantiomeric lactams (±)-**1d** carried out with α-CT afforded the corresponding compounds **2d** as a racemic form.[21] The corresponding molecular modeling evidences can be helpful in rationalizing this non-enantioselective behavior of these protease towards unsubstituted β-methoxy-γ-lactams.

Docking of the (*S*)- and (*R*)-**1d** enantiomers to α-CT revealed that both molecules are easily located in the protein active site, without significant steric interactions. Accordingly, the difference between bound and unbound state of the lactams is equal to 0.10 kcal/mol for (*S*)-**1d** and to 0.24 kcal/mol for (*R*)-**1d**, respectively. The relevant, optimized models of both α-CT/lactam complexes are reported in Fig. 6(a) and (b).

A detailed inspection of the corresponding molecular trajectories reveals that both molecules basically adopt a similar orientation within the active site, filling it downward from Ser 195 for 7.2 Å in the case of (*S*)-**1d**, and 6.5 Å in the case of the alternative isomer. Again, the amino acids forming the catalytic triad have the spatial orientation characterized by the presence of the three H-bonds described previously. Further, in the case of (*S*)-**1d**, the *o*-methoxy group interacts closely with the NH of the peptide bond between Asp 194 and Ser 195 (ADL = 2.42 Å), whilst the carbonyl of the lactam ring is engaged in stable H-bridging with the OH of Ser 190 (ADL = 2.39 Å). Finally, the nitrogen atom of the heterocycle is located in a favorable position to interact with the NH group of the peptidic bond between Val 213 and Ser 214, forming an H-bond of average dynamic length equal to 2.14 Å. In the case of the alternative enantiomeric complex, the oxygen of the OCH_3 group is again hydrogen-bonded with the NH group of the peptide bond between Asp 194 and Ser 195 (ADL = 2.10 Å) but also, alternatively, with the same group of the peptidic bond between Met 192 and Gly 193 (ADL = 2.38 Å). Lastly, the lactam C=O group interacts with the hydroxyl chain substituent of Ser 190, originating an H-bond of average dynamic length equal to 2.80 Å. All these stabilizing interactions reflect in the corresponding values of the residue-based decomposition of the non-bonding interaction energies listed in Table 7.

The results from the energetic analysis of 400 equally spaced snapshots taken from the MD simulation of the α-CT/(*S*)/(*R*)-**1d** complexes are summarized in Table 8. As can be clearly seen from Table 7, the calculated free energies of the α-CT/(*S*)-**1d** complex formation (ΔG_{bind} = −5.7 kcal/mol) and of the α-CT/(*R*)-**1d** complex formation (ΔG_{bind} = −5.9 kcal/mol) are almost equal, in harmony with the experimentally verified non-enantioselectivity of this protease with respect to unsubstituted β-carbomethoxy-γ-lactams. Accordingly, the components of the free energy of binding for one

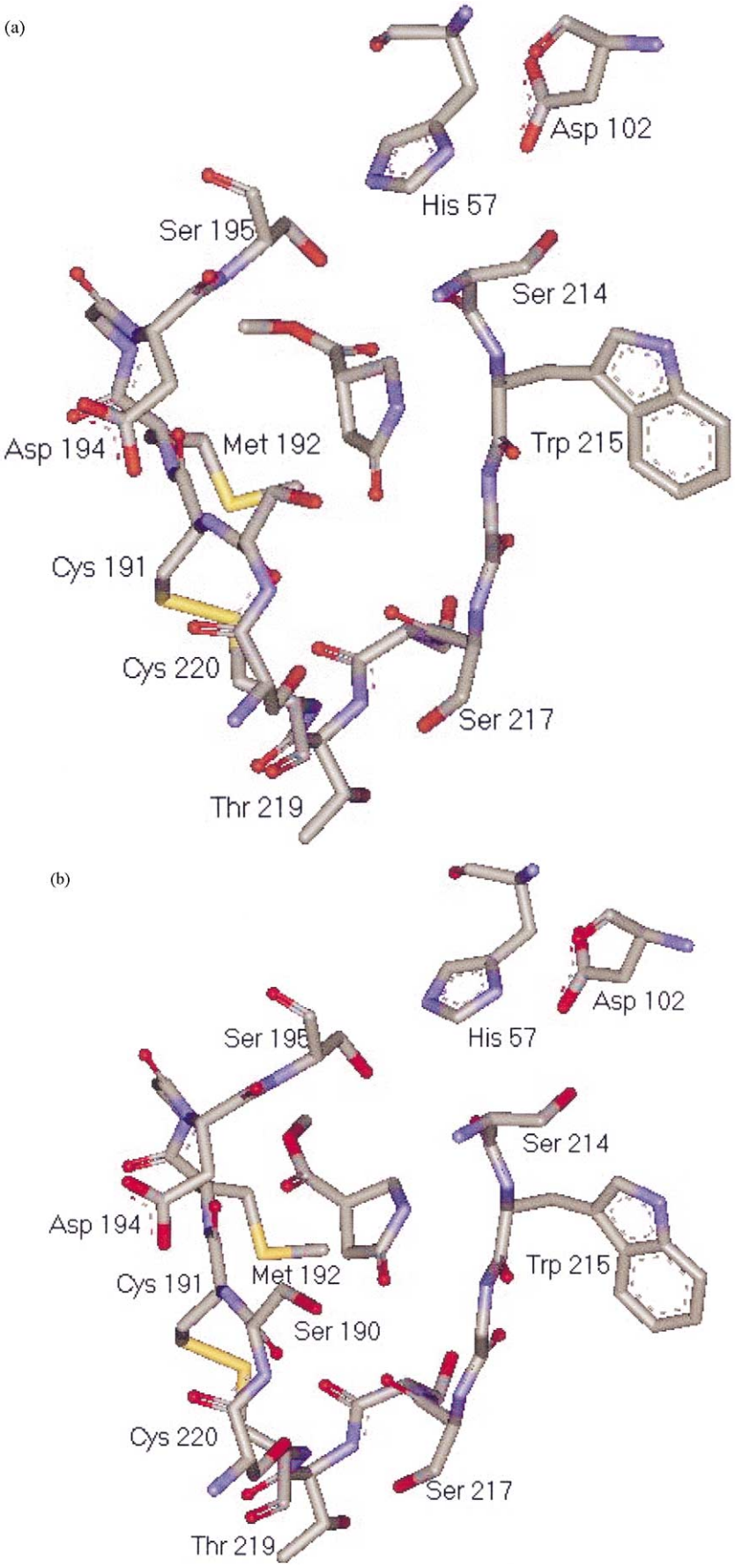

Figure 6. Optimized molecular model of the docked α-CT/(*S*)-**1d** (a) and α-CT/(*R*)-**1d** (b) complexes. For the sake of simplicity, only the amino acids forming the catalytic triad (His 57, Asp 102, and Ser 195), as well as those pertaining to the binding site are shown. Hydrogen atoms are also omitted for clarity.

Table 8. Energy terms and binding free energies[a] (kcal/mol) for the lactam enantiomers (*S*)/(*R*)-**1c** with α-CT

	(*S*)-**1d**	(*R*)-**1d**
ΔG^{vdW}_{int}	−8.1±0.1	−8.1±0.1
ΔG^{ele}_{intl}	−75.2±0.1	−75.0±0.1
ΔG_{MM}	−83.3	−83.1
ΔG^{np}_{sol}	−2.0±0.0	−1.9±0.0
ΔG^{ele}_{sol}	79.6±0.1	79.1±0.1
ΔG_{sol}	77.6±0.1	77.2±0.1
ΔG^{ele}_{tot}	2.4	2.2
ΔG_{bind}	−5.7	−5.9

[a] $T\Delta S$ not included (see text).

complex are essentially the same as those of the corresponding, alternative complex. This result is again not surprising, since the relative position, and the number and type of intermolecular interactions developed by each lactam enantiomer within the protein active site are equivalent.

4. Conclusions

The interaction of four enantiomeric couples of β-carbomethoxy-γ-lactams (±)-**1a**–**d** with the α-chymotrypsin active site has been simulated using a fine-tuned automated docking procedure, subsequently refined by quenched molecular dynamics. Further, to investigate the molecular basis of α-CT towards the experimentally verified enantioselective hydrolysis of this series of compounds,[21] with a combination of molecular mechanics energy derived from MD simulations in explicit solvent, and solvation free energy derived from a continuum solvation model, we have calculated reasonable absolute free energies of binding for all α-CT/enantiomer complexes formation.

In general, the energetic analysis reveals that the van der Waals interactions and the nonpolar contributions to solvation always provide the basis for the favorable absolute free energy of binding. On the other hand, a delicate balance exists between the always favorable gas-phase electrostatics term and the unfavorable change in electrostatic contribution to the solvation. Indeed, by counteracting the favorable electrostatic interactions that form between the lactam and the protein binding site, the desolvation of the protein residues plays an important role in determining the effect of the electrostatics, as a whole, on the formation of the α-CT/lactam enantiomer complex.

The results obtained from this study suggest that, in the case of enantioselective hydrolysis of lactams (±)-**1a**–**d** by α-CT, the combining site geometry appears to be reorganized in a manner that optimizes the electrostatics. Thus, in the design and optimization of further prodrugs based on this molecular skeleton, to be enantioselectively resolved via hydrolysis with α-CT, we should consider the electrostatics and the dispersion forces as well as the specific arrangement of hydrogen bonds. The optimization can involve minimizing the desolvation penalty for favorable electrostatic interactions. Thus, it is likely that molecular design efforts will benefit from effective strategies for optimizing electrostatics, including desolvation, as well as for developing reliable methods for creating ideal hydrogen bonding or van der Waals interactions which might improve further the enantioselective hydrolysis of this family of compounds by α-chymotrypsin.

Acknowledgements

The authors thank M. M. Garrett Morris and Peter J. Goodford for provision of the Software Autodock v. 3.0. While sadly remembering Peter A. Kollman, we are also much indebted to his group at UCSF (especially to Jim Caldwell) for providing us with Amber 6.0. This work was supported financially by the Italian Ministery for University and Research (MIUR, Rome, Italy, PRIN 2001 to S.P.) and by the University of Trieste (Trieste, Italy, Special Grant for Research to S.P. and M.F.). Both are gratefully acknowledged.

References

1. Wong, C.-H.; Whitesides, G. M. *Enzymes in Synthetic Organic Synthesis*; Elsevier: Oxford, 1994.
2. Schneider, M. P. *Enzymes as Catalysts in Organic Synthesis*; Reidel: Dordrecht, 1986.
3. DeSantis, G.; Jones, J. B. *Acc. Chem. Res.* **1999**, *32*, 99–107.
4. Kazlauskas, R. J. *Curr. Opin. Chem. Biol.* **2000**, *4*, 81–88.
5. Weissfloch, A. N. E.; Kazlauskas, R. J. *J. Org. Chem.* **1995**, *60*, 6959–6969.
6. Tuomi, W. V.; Kazlauskas, R. J. *J. Org. Chem.* **1999**, *64*, 2638–2647.
7. Kazlauskas, R. J.; Weissfloch, A. N. E.; Rappaport, A. T.; Cuccia, L. A. *J. Org. Chem.* **1991**, *56*, 2656–2665.
8. Holmquist, M.; Hæffner, F.; Norin, T.; Hult, K. A. *Protein Sci.* **1996**, *5*, 83–88.
9. Roberts, S. M. *Phil. Trans. R. Soc. Lond. B* **1989**, *324*, 557–587.
10. Berman, H. M.; Westbrook, J.; Feng, Z.; Gilliland, G.; Bhat, T. N.; Weissig, H.; Shindyalov, I. N.; Bourne, P. E. *Nucleic Acids Res.* **2000**, *28*, 235–242.
11. Tsukada, H.; Blow, D. M. *J. Mol. Biol.* **1985**, *184*, 703–711.
12. Birtktoft, J. J.; Blow, D. M. *J. Mol. Biol.* **1972**, *68*, 187–240.
13. Blow, D. M. *Isr. J. Chem.* **1974**, *12*, 483–493.
14. Gillan, T.; Mor, G.; Pepper, F. W.; Cohen, S. G. *Bioorg. Chem.* **1977**, *6*, 329–340.
15. Hanessian, S.; Reinhold, U.; Ninkovic, S. *Tetrahedron Lett.* **1996**, *37*, 8967–8970.
16. Ghelfi, F.; Bellesia, F.; Forti, L.; Ghirardini, G.; Grandi, R.; Libertini, E.; Montemaggi, M. C.; Pagnoni, U. M.; Pinetti, A.; De Buyck, L.; Parson, A. F. *Tetrahedron* **1999**, *55*, 5839–5852.
17. Galeazzi, R.; Mobbili, G.; Orena, M. *Tetrahedron* **1996**, *52*, 1069–1084.

18. Moody, C. M.; Young, D. W. *Tetrahedron Lett*. **1994**, *35*, 7277–7280.
19. Bergmann, R.; Gericke, R. *J. Med. Chem*. **1990**, *33*, 492–504.
20. Nilsson, B. M.; Ringdhal, B.; Hacksell, U. A. *J. Med. Chem*. **1990**, *33*, 580–584.
21. Felluga, F.; Pitacco, G.; Prodan, M.; Pricl, S.; Visintin, M.; Valentin, E. *Tetrahedron: Asymmetry* **2001**, *12*, 3241–3249.
22. Forzato, C.; Nitti, P.; Pitacco, G.; Valentin, E. *Targets in Heterocyclic Systems, Chemsitry and Properties*; Attanasi, O.; Spinelli, D., Eds.; S.C.I. 1999; Vol. 3, pp. 93–115.
23. Dembélé, Y. A.; Belaud, C.; Villiéras, J. *Tetrahedron: Asymmetry* **1992**, *3*, 511–514.
24. Morris, G. M.; Goodsell, D. S.; Halliday, R. S.; Huey, R.; Hart, W. E.; Belew, R. K.; Olson, A. J. *J. Comput. Chem*. **1998**, *19*, 1639–1662.
25. Case, D. A.; Pearlman, D. A.; Caldwell, J. W.; Cheatham, T. E., III; Ross, W. S.; Simmerling, C. L.; Darden, T. A.; Merz, K. M.; Stanton, R. V.; Cheng, A. L.; Vincent, J. J.; Crowley, M.; Tsui, V.; Radmer, R. J.; Duan, Y.; Pitera, J.; Massova, I.; Seibel, G. L.; Singh, U. C.; Weiner, P. K.; Kollman, P. A. *AMBER 6*, 1999, University of California, San Francisco, USA.
26. Pearlman, D. A.; Case, D. A.; Caldwell, J. W.; Ross, W. S.; Cheatham, T. E., III; DeBolt, S.; Ferguson, D.; Seibel, G. L.; Kollman, P. A. *Comp. Phys. Commun*. **1995**, *91*, 1–41.
27. *Cerius*^{2} Program Package, Accerlys Inc. San Diego, CA, USA.
28. Discover Program Package, Accelrys Inc. San Diego, CA, USA.
29. Frigerio, F.; Coda, A.; Pugliese, L.; Lionetti, C.; Menegatti, E.; Amiconi, G.; Schnebli, H. P.; Ascenzi, P.; Bolognesi, M. *J. Mol. Biol*. **1992**, *225*, 107–123.
30. Cornell, W. D.; Cieplak, P.; Bayly, C. I.; Gould, I. R.; Merz, K. M., Jr.; Ferguson, D. M.; Spellmeyer, D. C.; Fox, T.; Caldwell, J. W.; Kollman, P. A. *J. Am. Chem. Soc*. **1995**, *117*, 5179–5197.
31. Jayaram, B.; Sprous, D.; Beveridge, D. L. *J. Phys. Chem. B* **1998**, *102*, 9571–9576.
32. Weiser, J.; Shenkin, P. S.; Still, W. C. *J. Comp. Chem*. **1999**, *20*, 217–230.
33. Fermeglia, M.; Pricl, S. *AIChE J*. **1999**, *45*, 2619–2627.
34. Bayly, C. I.; Cieplak, P.; Cornell, W. D.; Kollman, P. A. *J. Phys. Chem*. **1993**, *97*, 10269–10280.
35. Delley, B. *J. Chem. Phys*. **1990**, *92*, 508–520.
36. Mehler, E. L.; Solmajer, T. *Protein Engng*. **1991**, *4*, 903–910.
37. Jorgensen, W. L.; Chandrasekhar, J.; Madura, J. D.; Impey, R. W.; Klein, M. L. *J. Comput. Phys*. **1983**, *79*, 926–935.
38. Darden, T.; York, D.; Pedersen, L. *J. Chem. Phys*. **1993**, *98*, 10089–10092.
39. Ryckaert, J. P.; Ciccotti, G.; Berendsen, H. J. C. *J. Comput. Phys*. **1977**, *23*, 327–341.
40. Berendsen, H. J. C.; Postma, J. P. M.; van Gunsteren, W. F.; DiNola, A.; Haak, J. R. *J. Comput. Phys*. **1984**, *81*, 3684–3690.
41. Srinivasan, J.; Cheatham, T. E., III; Cieplak, P.; Kollman, P. A.; Case, D. A. *J. Am. Chem. Soc*. **1998**, *120*, 9401–9409.
42. Sharp, K. A.; Honig, B. H. *Annu. Rev. Biophys. Chem*. **1990**, *19*, 301–312.
43. Chong, L. T.; Duan, Y.; Wang, L.; Massova Kollman, P. A. *Proc. Natl. Acad. Sci*. **1999**, *96*, 14330–14335.
44. Sitkoff, D.; Sharp, K. A.; Honig, B. H. *J. Phys. Chem*. **1994**, *98*, 1978–1988.
45. Gilson, M. K.; Sharp, K. A.; Honig, B. H. *J. Comput. Chem*. **1987**, *9*, 327–335.
46. Sanner, M. F.; Olson, A. J.; Spehner, J. C. *Biopolymers* **1996**, *38*, 305–320.
47. Kuhn, B.; Kollman, P. A. *J. Med. Chem*. **2000**, *43*, 3786–3791.
48. Connolly, M. L. *Science* **1983**, *221*, 709–713.
49. Connolly, M. L. *J. Am. Chem. Soc*. **1985**, *107*, 1118–1124.
50. Fermeglia, M.; Pricl, S. *Fluid Phase Eq*. **1999**, *158*, 49–58.
51. Fermeglia, M.; Ferrone, M.; Pricl, S.; Spada, P. *Food Hydrocoll*. **2002**, in press.
52. Fermeglia, M.; Ferrone, M.; Manfredini, M.; Porcu, L.; Pricl, S. *J. Med. Chem*. **2002**, submitted.
53. Novotny, J.; Sharp, K. A. *Progr. Biophys. Mol. Biol*. **1992**, *58*, 203–224.
54. Misra, V. K.; Sharp, K. A.; Friedman, R. A.; Honing, B. H. *J. Mol. Biol*. **1994**, *238*, 245–263.
55. Misra, V. K.; Hecth, J. L.; Sharp, K. A.; Friedman, R. A.; Honing, B. H. *J. Mol. Biol*. **1994**, *238*, 264–280.
56. Sharp, K. A. *Biophys. Chem*. **1996**, *61*, 37–49.
57. Shen, J.; Wendoloski, J. *J. Comput. Chem*. **1996**, *17*, 350–357.
58. Novotny, J.; Bruccoleri, R. E.; Davis, M.; Sharp, K. A. *J. Mol. Biol*. **1997**, *268*, 401–411.
59. Bruccoleri, R. E.; Novotny, J.; Davis, M. E. *J. Comput. Chem*. **1997**, *18*, 268–276.
60. Mares-Guia, M.; Figueiredo, A. F. S. *Biochemistry* **1970**, *9*, 3223–3227.
61. Mares-Guia, M.; Nelson, D. L.; Rogana, E. *J. Am. Chem. Soc*. **1977**, *99*, 2331–2336.